Eur Biophys J (2001) 29: 597–606
DOI 10.1007/s002490000110

ARTICLE

**Giuseppe Chirico · Maddalena Collini · Katalin Tóth**
**Nathalie Brun · Jörg Langowski**

# Rotational dynamics of curved DNA fragments studied by fluorescence polarization anisotropy

Received: 6 April 2000 / Revised version: 9 August 2000 / Accepted: 8 September 2000 / Published online: 18 November 2000


**Abstract** The rotational dynamics of short DNA fragments with or without intrinsic curvature were studied using time-resolved phase fluorimetry of intercalated ethidium with detection of the anisotropy. Parameters determined were the spinning diffusion coefficient of the DNA fragments about the long axis and the zero-time ethidium fluorescence anisotropy. We find a significant decrease in the spinning diffusion coefficient for all curved fragments compared to the straight controls. This decrease is likewise evident in rotational diffusion coefficients computed from DNA structures obtained by a curvature prediction program for these sequences. Using a hinged-cylinder model, we can identify the change in rotational diffusion coefficient with a permanent bend of 13–16° per helix turn for the sequences studied. Moreover, for some of the curved fragments an increased flexibility has to be assumed in addition to the permanent bend in order to explain the data.

**Key words** DNA torsional rigidity · DNA bending · Phase fluorimetry · Curvature prediction

## Introduction

Sequence-dependent structure variations of DNA, in particular DNA curvature, play an important role in the organization and function of the genome. It is known, for instance, that DNA curves can organize the global structure of superhelical DNA (Laundon and Griffith 1988; Pfannschmidt and Langowski 1998; Tsen and Levene 1997), and that curved segments participate in transcriptional regulation (Bracco et al. 1989; Griess et al. 1993; Kim et al. 1995; Längst et al. 1997; Lavigne et al. 1992; Ohyama 1996; Perez-Martin et al. 1994; Rojo and Salas 1991). The possibility of DNA curvature was first proposed by Trifonov and Sussman (1980), who pointed out that local kinks in phase with the helical repeat would cause the DNA helix axis to follow a globally bent path.

DNA curvature is generally measured by gel migration anomaly (GMA), i.e. the slower migration of a curved DNA fragment in a polyacrylamide gel relative to a straight fragment of the same size. The sequences that cause GMA when repeated in phase with the helix pitch are quite well known: the most prominent example is $A_n$ with $n \geq 4$. While GMA is an important tool for characterizing curved DNA in a semiquantitative way, the quantitative interpretation of GMA data in terms of DNA curvature angle or flexibility is difficult because the mobility of the DNA chain in the gel is restricted.

Several groups have studied the conformation of curved DNA free in solution: electric dichroism measurements on 267 bp DNA restriction fragments from the kinetoplast of *Leishmania tarentolae* (Levene et al. 1986) at rather low ionic strength (1.6 mM NaCl) showed a 20% difference in rotational relaxation times between two fragments which had a curve either in the center or near the end of the molecule. Later, electric dichroism data by Pörschke et al. (1993) could not confirm a strong curvature on 161–399 bp DNA fragments from *Chironomus thummi thummi* either at low or at physiological salt concentrations, although they showed a high gel migration anomaly. These results suggested an increased rigidity combined with only a slight curvature. The increased rigidity was also confirmed by Levene et al. (1986). Recently, end-to-end distances for a 31 bp curved DNA and a straight DNA of the same length were measured using fluorescence resonance energy transfer (FRET). The change in end-to-end distance was interpreted as a curvature angle of

K. Tóth (✉) · N. Brun · J. Langowski
Deutsches Krebsforschungszentrum,
Division Biophysics of Macromolecules,
Im Neuenheimer Feld 280, 69120 Heidelberg, Germany
E-mail: joerg.langowski@dkfz-heidelberg.de
Tel.: +49-6221-423390; Fax: +49-6221-423391

G. Chirico · M. Collini
Istituto Nazionale di Fisica per la Materia,
Università degli Studi di Milano Bicocca,
Via Celoria 16, 20133 Milan, Italy

$23 \pm 3°$ per helical turn for an $A_6$ sequence at 10 mM NaCl, and the curvature was found to increase with salt concentration (Tóth et al. 1998).

In spite of the observed changes in DNA rigidity, the question of how much of the DNA curvature is due to changes in the equilibrium static structure, i.e. a minimum of the bending potential at a non-zero bending angle, and how much is due to anisotropic flexibility remains unresolved. Studies of the dynamics of DNAs with curved and non-curved sequences might help to understand this problem. One method that has been used to study the internal dynamics and the rotational diffusion of DNA is the fluorescence polarization anisotropy (FPA) decay of intercalated ethidium, which probes the local rotational dynamics of the DNA (Barkley and Zimm 1979; Collini et al. 1995; Thomas et al. 1980; Wu et al. 1987). Since the rotational diffusion coefficient of an elongated object about its long axis ($D_{spin}$) is inversely proportional to the square of the hydrodynamic radius about that axis, static curvature or other deviations from a straight cylinder shape should manifest themselves in a decrease of $D_{spin}$. In addition, FPA is sensitive to the internal motions of the DNA chain and has been used extensively to study the torsional elasticity of DNA (for a review, see Schurr et al. 1992). Sites of local torsional weakness, such as bulge loops, have been shown to influence the FPA decay in a characteristic way (Collini et al. 1998).

In this work, we use FPA in a phase fluorimeter to study the structure and dynamics of short (30–111 bp) DNA fragments, some of which contain sequences that are predicted to be curved and that show GMA. We show that phased A-tracts that cause GMA do also increase the apparent hydrodynamic radius of the DNA, consistent with the assumption of a permanent curvature. Furthermore, we can show that the sequence influences the local twisting dynamics; for some of the DNAs, an internal joint of lower torsional rigidity has to be assumed in order to fit the data.

## Materials and methods

### DNA fragments

DNA fragments with lengths in the range 30–111 base pairs were prepared either by synthesis (Interactiva Biotechnologie, Ulm, Germany, or in-house) or from plasmids by restriction cleavage and HPLC purification. Fragments with sequences predicted to give a curved structure are labeled as C*n*, where *n* is the length in base pairs. Fragments predicted to be straight are called S*n* (see Results and Table 1). Fragments prepared by restriction digestion from plasmids are labeled with the letter p: S*n*p. The fragments S80p and S106p were isolated from a *Hae*III/*Hin*fI digest of the plasmid p1868 (Hammermann et al. 1997). S100p and C111p were prepared by *Eco*RI/*Hin*dIII digestion of the plasmids pUC18/3A and pUC18/4A, respectively (Kremer et al. 1993). The lengths and average AT contents are listed in Table 1.

The first pair of fragments studied (S100p and C111p) were sequences examined earlier as part of longer fragments with different gel mobilities (Diekmann 1986). Sequence differences are highlighted below:

S100p: **5′**-AATTCTCATG TTTGACAGCT TATCAT (GA-C**AAAG**CTC)$_7$ GATA-**3′**
C111p: 5′-AATTCTCATG TTTGACAGCT TATCAT**C** (GAC**AAAA**CTC)$_8$ GATA-**3′**

In order to minimize the difference in the base composition of the fragments to be compared, we also had the following pair of fragments synthesized:

S100: 5′-GGGCCGCCCG (G**AC**AAAGCTC)$_8$ GGGCCGC-CCG-3′
C100: 5′-GGGCCGCCCG (G**CA**AAAGCTC)$_8$ GGGCCGC-CCG-3′

The common characteristic of these sequences is the repetition of adenine bases in phase with the helical pitch of the DNA. It is known that A-tracts longer than 3A lead to anomalously slow migration in polyacrylamide gel electrophoresis. A pair of shorter fragments with stronger relative curvature was also constructed:

S31: 5′-C**TATATA**CGG CG**TATATA**CGG C**TATATA**-CGG-3′
C31: 5′-C**AAAAAA**CGG CG**AAAAAA**CGG C**AAAAAA**C-GG-3′

In order to compare DNAs with different lengths and from different preparations, fragments without repetitive sequences were prepared from plasmids (S80p, S106p); S80 with the same sequence as S80p was also synthesized:

S80, S80p: **5′**-GGCCCCAGTG CTGCAATGAT ACCGC-GAGAC CCACGCTCAC CGGCTCCAGA TTTATCAGCA ATAAACCAGC CAGCCGG-AAG-3′
S106p: 5′-GAGTCCAACC CGGTAAGACA CGACTTA-TCG CCACTGGCAG CAGCCACTGG TAA-CAGGATT AGCAGAGCGA GGTATGTAGG CGGTGCTACA GAGTTCTTGA AGTGGT-3′

Fragments obtained through restriction presented in some cases sticky ends: this is indicated by bold italics on the respective ends.

All fragments were HPLC purified (Merck LiChroSpher 4000 DMAE, with solvents containing acetonitrile, KCl, and phosphate buffer), concentrated by vacuum centrifugation, and desalted through a NAP5 column (Pharmacia) into 10 mM Na-cacodylate buffer at pH 7.5. DNA concentrations varied between 0.05 and 0.5 mg/mL. For the FPA measurements, ethidium bromide was added to achieve a ratio of one ethidium per 200 bp. FPA measurements were done in quartz cuvettes with an optical length of 0.3 cm at 25 °C.

Purity, length, and mobility of the samples were controlled by gel electrophoresis on 12% polyacrylamide gels in TBE buffer at a field strength of about 10 V/cm for about 3 h at a temperature of 34 °C. Gels were observed by UV illumination after ethidium staining. Thermal melting curves of the DNA fragments in solution were recorded by absorbance at 260 nm on a Cary 4E spectrophotometer (Varian, Mulgrave, Australia) equipped with a Peltier thermoregulator. The heating rate was 0.2 °C/min in the temperature range 25–95 °C. Circular dichroism spectra of the samples were measured in 1 mm quartz cuvettes on a Jasco 520 spectropolarimeter in the 220–320 nm region using a DNA concentration of 0.5–1 mg/mL at 25 °C.

### Fluorescence polarization anisotropy

FPA decay measurements were obtained with a frequency domain K2-ISS (Urbana, Ill., USA) fluorimeter operating at modulation frequencies between 1 and 40 MHz. The excitation light was the green 514.5 nm output of an argon ion laser (Spectra Physics 2025) at a power of 500–700 mW; for further details see Collini et al. (1992). Digital data acquisition and storage were provided by the ISS-A2D ACD card inserted in a personal computer. For each set of data, 25 logarithmically spaced frequencies were employed in the range 1–40 MHz with a cross-correlation frequency of 80 Hz. A

550 nm long-pass filter was used to separate the scattered excitation light. The temperature was kept at $T = 24.5$ °C by a recirculating thermostat and directly checked by a thermocouple inserted in the cell compartment.

Data were analyzed using a Fortran routine minimizing $\chi^2$ for phases and modulations according to the Marquardt algorithm (Collini et al. 1995). The ethidium fluorescence lifetimes were measured for some of the samples and always found to be very close to 22.5 ns and at 1.8 ns for bound and free dye, respectively. The trial phase differences and modulation ratios were the Laplace transform of the fluorescence intensities obtained from a theoretical expression of $r(t)$ for the straight or curved cylinder, or the flexible joint model (see eq. 1 in Collini et al. 1995). We computed the relaxation times of the internal motions according to a fixed value of the local hydrodynamic radius $R = 9.5$ Å, i.e. the consensus value for the DNA B-helix (Eimer and Pecora 1991; Fujimoto et al. 1994). Unless otherwise explicitly stated, the persistence length, $P_{\mathrm{dyn}}$, and the torsional constant, $\alpha$, have been kept at $P_{\mathrm{dyn}} = 200$ nm and $\alpha = 8 \times 10^{-12}$ erg (1 erg $= 10^{-7}$ J) according to recent experimental results (Song and Schurr 1990). In order to account for curved DNA structures we used the global hydrodynamic radius, $R_{\mathrm{h}}$, as a fitting parameter in the computation of the spinning and tumbling diffusion coefficients of DNA. Further fitting parameters were the limiting anisotropy, $r_0$, and the fraction $x_{\mathrm{f}}$ of free ethidium.

## Theory

### FPA decay

In the following, we briefly review the theory of the FPA of ethidium intercalated into DNA as measured in a phase fluorimeter. The measured fluorescence anisotropy, $r(t)$, is the normalized difference between the fluorescence decays detected for polarizations parallel, $I_{\parallel}(t)$, and perpendicular, $I_{\perp}(t)$, to the vertical polarization of the exciting beam:

$$r(t) = \big(I_{\parallel}(t) - I_{\perp}(t)\big)\big(I_{\parallel}(t) + 2I_{\perp}(t)\big)^{-1} \tag{1}$$

With the exception of very short times ($\leq 1$ ns) when wobbling may occur, the ethidium probe can be considered firmly bound, thereby suffering the same type of diffusive motions as the host macromolecule. Within this approximation, the probe anisotropy is reporting the DNA internal and overall diffusive motions.

At length scales greater than a few base pairs, DNA can be regarded as a flexible elastic filament with mean cylindrical symmetry and a straight equilibrium structure. When the dye wobbling is uncoupled from the torsional and bending motions of DNA, the expression of the FPA is given as a product of several contributions (Schurr 1984):

$$r(t) = r_0 \sum_{n=-2}^{2} I_n(t) C_n(t) F_n(t) \exp\big(-n^2 D_{\mathrm{S}} t\big) \times \exp\big(-\big(6 - n^2\big) D_{\mathrm{T}} t\big) \tag{2}$$

The internal correlation functions $I_n(t)$ depend on the angle $\varepsilon_0$ between the dye transition dipole and the polymer axis of symmetry (e.g., $\varepsilon_0 = 70.5°$ for ethidium). They are essentially time independent since the wobbling relaxation time (of the order of a few picoseconds) is below the time resolution of our FPA setup. However, wobbling manifests itself in a limiting anisotropy factor $r_0 < 0.4$, which would be the theoretical maximum for an immobile fluorophore at random orientation. $C_n(t)$ represents the internal twisting correlation function:

$$C_n(t) = \exp\Big[-n^2\Big\langle \Delta\phi_{\mathrm{T}}(t)^2 \Big\rangle\Big] \tag{3}$$

where $\Delta\phi_{\mathrm{T}}(t)$ is the torsional displacement of the subunits around their $z$-axes (here identified as the long symmetry axis of the cylinder). $F_n(t)$ are the correlation functions of the internal bending motions:

$$F_n(t) = \exp\Big[-\big(6 - n^2\big)\Big\langle \Delta\phi_{\mathrm{B}}(t)^2 \Big\rangle\Big] \tag{4}$$

where $\Delta\phi_{\mathrm{B}}(t)$ is the bending angular displacement perpendicular to the helix axis. Explicit expressions of the average square angular displacements can be found in Schurr (1984) and depend on the DNA dynamic persistence length, $P_{\mathrm{dyn}}$, its torsional elastic constant, and on the local hydrodynamic radius, $R$. The dynamic persistence length is the contribution to the total persistence length $P$ that is due to Brownian deformations of the chain. In general, the persistence length of DNA can be thought to consist of three contributions (Song and Schurr 1990):

$$\frac{1}{P} = \frac{1}{P_{\mathrm{S}}} + \frac{1}{P_{\mathrm{slow}}} + \frac{1}{P_{\mathrm{dyn}}} \tag{5}$$

where $P_{\mathrm{S}}$ is the persistence length due to sequence-dependent deviation from the ideal straight B-DNA structure, $P_{\mathrm{slow}}$ is the contribution due to slow structure variations on the time scales $> 1$ ms, and $P_{\mathrm{dyn}}$ is the contribution due to local elastic deformation that relax on faster time scales. $P_{\mathrm{dyn}}$ has been estimated to ~210 nm (Song and Schurr 1990).

The leading terms in $r(t)$ corresponding to the rigid body spinning and tumbling rotation are related to the diffusion coefficients for the spinning, $D_{\mathrm{S}}$, and tumbling, $D_{\mathrm{T}}$, DNA helix motions. They can be computed, for a straight cylindrical DNA fragment, according to relations given by Tirado and Garcia de la Torre (1980):

$$D_T = \frac{3k_BT[\ln(p) + \delta_T]}{\pi\eta L^3} \qquad D_S = \frac{k_BT}{3.841\pi\eta LR^2(1 + \delta_s)} \tag{6}$$

where $p$ is the DNA axial ratio, $\eta$ is the solution viscosity, $T$ the temperature, and $\delta_{\mathrm{S}}$ and $\delta_{\mathrm{T}}$ are correction factors which take into account the finite length of the DNA and depend on its axial ratio. For DNA fragments with slight deviations from a straight equilibrium, one expects little variation in $D_{\mathrm{T}}$, since the end-to-end distance does not change very much; $D_{\mathrm{S}}$, however, should be significantly slower because the average expanse of the DNA about the long axis of rotation increases.

In the presence of a small free dye contribution, the total anisotropy is given by the intensity-weighted average of the bound and of the free fluorophore

(Lakowicz 1983). The free dye anisotropy is given by:

$$r_F(t) = r_0 \exp(-t/\tau_{rot}) \quad (7)$$

where $\tau_{rot}$ is taken to be 100 ps and $r_0 = 0.4$ (Collini et al. 1992).

The above model corresponds to a DNA with uniform dynamic properties along the chain. Unfortunately, no analytical theories are available for non-uniform chains, and one must resort to numerical Brownian dynamics simulations in many cases. An approximate and simplified model for short non-uniform chains can be a flexible joint, where the fragment is envisioned as a couple of rods connected by a harmonic torsional spring. Additional internal motions in the two rods can be considered separately in the limit of high internal coupling of the two arms. This simplified model has been already used successfully for the analysis of the FPA spectra of bulged DNAs (Collini et al. 1998). The modifications to the FPA decay that can be considered are then:

$$r(t) = r_0 \sum_{n=0}^{2} C_{J,n}(t) C_n(t) F_{J,n}(t) F_n(t) \exp\left(-n^2 D_S t\right) \times \exp\left(-\left(6-n^2\right) D_T t\right) \quad (8)$$

where the functions $C_n(L,t)$ and $F_n(L,t)$ are the torsional and bending anisotropy contributions due to the internal dynamics of each half of the molecule of total length $L$. The contributions $C_{J,n}(t)$ and $F_{J,n}(t)$ arise from the joint dynamics (Schurr 1984):

$$C_{J,n}(t) = \exp\left(-n^2 \left\langle \Delta\phi_T(t)^2 \right\rangle\right) \quad (9)$$

and

$$F_{J,n}(t) = \exp\left(-\left(6-n^2\right) \left\langle \Delta\phi_B(t)^2 \right\rangle\right) \quad (10)$$

Their mean square displacements can be written as (Doi and Edwards 1986):

$$\left\langle \Delta\phi_B(t)^2 \right\rangle = 2\sigma_B^2 (1 - \exp(-t\Gamma_B)) \quad (11)$$

and

$$\left\langle \Delta\phi_T(t)^2 \right\rangle = 2\sigma_T^2 (1 - \exp(-t\Gamma_T)) \quad (12)$$

where the two relaxation rates $\Gamma_B$ and $\Gamma_T$ are related to the variance of the angular displacements $\sigma_B$ and $\sigma_T$ and to the spinning and tumbling diffusion coefficients $D^0_{SPIN}$ and $D^0_{TUMB}$ of the two DNA halves as $\Gamma_T = D^0_{SPIN}/\sigma_T^2$ and $\Gamma_B = D^0_{TUMB}/\sigma_B^2$.

The FPA data shown in the Results section are obtained by detecting the FPA decay in the frequency domain (Lakowicz and Maliwal 1985; Weber 1977). A radiofrequency (MHz) modulated excitation beam forces the fluorescence emission to be modulated at the same frequency, but phase shifted with respect to the excitation and reduced in its relative amplitude (demodulation). The phase shifts and modulations are recorded at each frequency for each polarization direction and then compared by computing the phase differences and the demodulation ratios:

$$\Delta\phi(\omega) = \phi_\perp(\omega) - \phi_\parallel(\omega) \qquad \Delta M(\omega) = M_\perp(\omega)/M_\parallel(\omega) \quad (13)$$

which are related to the Laplace transform of the intensity decays at the two polarization conditions, $L(I_\perp, I_\parallel)(\omega)$, in the following way (Lakowicz 1983):

$$\frac{L(I_\perp)(\omega)}{L(I_\parallel)(\omega)} = \Delta M(\omega) \exp[i\Delta\phi(\omega)] \quad (14)$$

We recall that $I_\parallel(t) = I_{tot}(1 + 2r(t))/3$ and $I_\perp(t) = I_{tot} \times (1 - r(t))/3$. In this way, the fluorescence anisotropy decay in the time domain (Eq. 2) can be related, through Eq. 13, to phase differences and demodulation ratios in the frequency domain (Collini et al. 1992). Owing to the Laplace transform that relates Eq. 2 to Eq. 13, the dependence of the measured frequency spectra on the DNA dynamical and structural parameters is not evident and must usually be inferred from numerical simulations.

## Prediction of the curvature and hydrodynamic properties of the DNA fragments

The three-dimensional trajectories of the helix axes of the studied sequences were predicted by our program *Curvature* (Schätz and Langowski 1997), using the set of wedge angles published by Bolshoy et al. (1991) (the program runs on Linux systems and is available through the authors upon request). The rotational diffusion coefficients of DNA fragments about the long axis (spinning) and about the short axis (tumbling) were determined by modeling the molecule as a stack of $N_r$ rings of radius $R_r$, each composed of $N_s$ touching spheres of radius $\sigma$ (Tirado and Garcia de la Torre 1979). The centers of the rings lie on the trajectory defined by the helix axis. The rotational diffusion coefficients were computed according to the general scheme given by García Bernal and García de la Torre (1980), where the small coupling between the translational and rotational diffusion coefficients is taken into account. The hydrodynamic equations were solved numerically as described earlier (Collini et al. 1995), obtaining the three eigenvalues of the rotational matrix. Two of these eigenvalues were always very close for short fragments (within 10% for kink angles $\theta < 70°$); therefore we averaged them in order to get the spinning diffusion coefficient, while the third one was interpreted as the tumbling diffusion coefficient. This computational approach has been checked previously on a 50 bp fragment (Collini et al. 1995), finding a 2–4% agreement with the smooth cylinder result. Diffusion coefficients of the 31 and 100 bp fragments were also computed

**Table 1** Characteristics of the DNA fragments used. Length, *N*, in base pairs, and AT content of the DNA fragments. A-rep indicates the number of adjacent A base pairs and the in-phase repetition number (in parentheses) in the sequence. The curvature angle is the angle between the ends of a circular arc fitted to the overall shape of the fragment calculated as described in the text. $R_h$ is the best fit hydrodynamic radius obtained from the complete FPA data with $\alpha = 8 \times 10^{-12}$ erg. The average value of the limiting anisotropy is $r_0 = 0.38 \pm 0.01$. The tumbling and spinning diffusion coefficients $D_T$ and $D_S$ were simulated as described in the text from the computed shape of the DNA fragments. The $D_T$ and $D_S$ values from a fit to the FPA data are given in the last section of the table

| Name | Bp | AT (%) | A-rep. | Curvature angle (°) | $R_h$ (Å) | Simulated | | | From fit to FPA data | | |
|---|---|---|---|---|---|---|---|---|---|---|---|
| | | | | | | $D_T$ (MHz) | $D_S$ (MHz) | $D_S/D_T$ | $D_T$ (MHz) | $D_S$ (MHz) | $D_S/D_T$ |
| S31 | 31 | 58 | 0 | 10.5 | 11.5 | 4.1 | 29.1 | 7 | 4.0 | 25.6 | 6 |
| C31 | 31 | 58 | (6) 3 | 149.1 | – | 4.5 | 16.4 | 4 | 3.7 | 20.9 | 6 |
| S80 | 80 | 41 | 0 | 40.6 | 9.2 | 0.3 | 9.0 | 32 | 0.4 | 13.2 | 30 |
| S80p | 80 | 41 | 0 | – | 9.3 | – | – | – | – | – | – |
| S100 | 100 | 40 | (3) 8 | 101.9 | 7.7 | 0.2 | 3.3 | 18 | 0.3 | 16.8 | 62 |
| C100 | 100 | 40 | (4) 8 | 201.8 | – | 0.4 | 1.5 | 4 | 0.2 | 11.1 | 45 |
| S100p | 100 | 57 | (3) 7 | 110.9 | 10.2 | 0.2 | 4.0 | 23 | 0.2 | 10.2 | 42 |
| S106p | 106 | 44 | 0 | 37.6 | 9.25 | – | – | – | – | – | – |
| C111p | 111 | 61 | (4) 8 | 196.3 | – | 0.2 | 1.2 | 6 | 0.2 | 6.6 | 38 |

from a simplified bent rod model for illustrating the effect of bending angle. Here the DNA radius is taken as $R_D = R_r + \sigma = 1$ nm, and $N_s = 10$. This leads to $\sigma = R_D \sin(\pi/N_s)/(1 + \sin(\pi/N_s)) = 0.236$ nm and $R_r = 0.764$ nm. The number of stacks for the 31 bp and the 100 bp fragments are $N_r = 23$ and 73, respectively. In order to avoid superposition of spheres at the kink, the two arms of the bent rod were slightly displaced along the axis of the half-rod. This leads to a negligible increase in the total contour length of the model.

For the evaluation of the diffusion coefficients of the actual DNA sequences investigated by FPA, we used the helix axis predicted by the *Curvature* program, on which we placed stacks of rings composed of four spheres ($N_s = 4$). In this case, $\sigma = R_D \sin(\pi/4)/(1 + \sin(\pi/4)) = 0.415$ nm when assuming $R_D = 1$ nm. The discreteness of the model results in a systematic underestimate of the contour length of the modeled fragments. Moreover, the displacement of some stacks of rings along the helix axis, at the sites of high curvature, leads to models slightly longer than the actual fragments. We estimate that these effects might give an uncertainty of about 20% in the ratio of the spinning to the tumbling coefficients.

We note also that a set of programs for computing the hydrodynamic properties of model objects consisting of spherical subunits exists in the public domain [HYDRO (Garcia de la Torre et al. 1994) and SOLPRO (Garcia de la Torre et al. 1997)]. These programs use essentially the same algorithms as described here.

## Results and discussion

### *Curvature* analysis of the DNA sequences

The three-dimensional structure of the nine fragments was predicted using our program *Curvature* (Schätz and Langowski 1997). Table 1 shows estimates of the bending angles which were obtained from the angle between the ends of a circular arc fitted to the overall shape of the fragment. Likewise, the table shows the spinning and tumbling diffusion coefficients calculated as shown in the Materials and methods section. It can be seen that the ratio of spinning to tumbling diffusion coefficients is much lower for the fragments with predicted curvature than for those predicted to be straight. This effect is even more striking for the longer fragments, since an increase of the $D_S/D_T$ ratio would be expected for a simple rigid-rod model. The dependence of the diffusion coefficients on the length, $L$, and radius, $R$, for a straight rod is $D_T \approx 1/L^3$ and $D_S \approx 1/(LR^2)$, and therefore the ratio $D_S/D_T$ should increase as $(L/R)^2$. The simulated ratios, on the contrary, are not changing appreciably with the DNA length for the curved fragments owing to their strong curvature. As shown below, the $D_S/D_T$ ratio *measured in solution* increases in general with DNA size for both straight and curved fragments. This is not only because the longer sequences tend to deviate from a straight line (see "bending angle" in Table 1) simply due to sequence variations, but also due to the thermal bending motion of the helix.

### Gel migration anomaly of the 100 bp sequences with phased A-tracts

We have compared the gel migration properties of our S100 and C100 fragments with 320 bp fragments studied earlier (Kremer 1992), which contained the same 80 bp repetitive sequences flanked by 160 and 80 bp of random DNA. From the gel pictures in Fig. 1 we determined the retardation of the curved fragments to 50% for the 320 bp and 4% for the 100 bp long fragments. For the 31 bp fragments, no significant retardation is detectable. Curved and straight 320 bp fragments were not distinguishable in FPA measurements (data not shown). However, the length of these DNAs being more than twice the persistence length (50 nm), we suppose that the structural effect of the curvature is masked by the overall flexibility of the fragment. In summary, the gel electro-

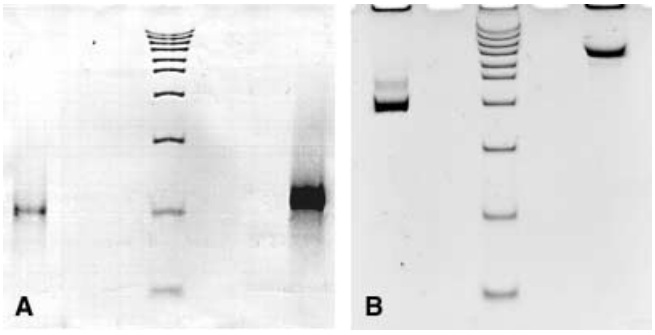


**Fig. 1** Demonstration of the anomalous gel migration behavior of fragments S100 (*left*, lane 1) and C100 (*left*, lane 3) in comparison with longer fragments containing the same repetitive sequences S320 (*right*, lane 1) and C320 (*right*, lane 3). Both gels were 12% polyacrylamide. The start of the *left* gel is marked by the *horizontal line*. Lanes 2 in both gels are Bio-Rad markers containing a ladder of 50, 100, 200, 300, 400, 500, 700, 1000, 1500, and 2000 bp DNA fragments. The photos are negative video images of the actual ethidium-stained fluorescent gels

phoresis experiments and the computer simulations indicate a subset of fragments that are expected to behave as straight cylinders (the S series) and another one (the C series) that should exhibit some degree of permanent curvature.

## Differences in the melting profile and CD spectra are not unambiguous signs of curved structure

In a series of papers, Chan and co-workers (Chan et al. 1990, 1993, 1997) have characterized differences in the thermal melting profile and the CD of DNAs containing or lacking oligo-A tracts. The sequences studied were poly(dA)·poly(dT) and repeats of $A_5$ blocks in phase with the helix repeat. They saw a rather broad pre-melting transition centered around 32 °C for the oligo-A containing sequences which they associated with a straightening of the sequence-induced bend.

In our case, the fragments S100 and C100 both have the same base composition and differ only by a dinucleotide inversion in eight positions; S100 has an $A_4$ and C100 an $A_3$ repeat. The thermal melting analysis and the CD spectra of these two fragments show large differences (Fig. 2); however, in contrast to the results by Chan et al., we find a much broader transition for the non-curved C100 fragment than for the curved S100 sequence. While CD and melting are sensitive to local structure differences, some global structural change must be present in order to explain the large differences. However, we see here that the presence of a pre-melting transition must not necessarily be correlated with the presence or absence of sequence-induced bending. A systematic study of sequence effects on CD spectra would be necessary to explore this problem completely, but this is outside the scope of the present paper. We note that such global effects of local sequence changes have been observed in other cases (Song et al. 1990).

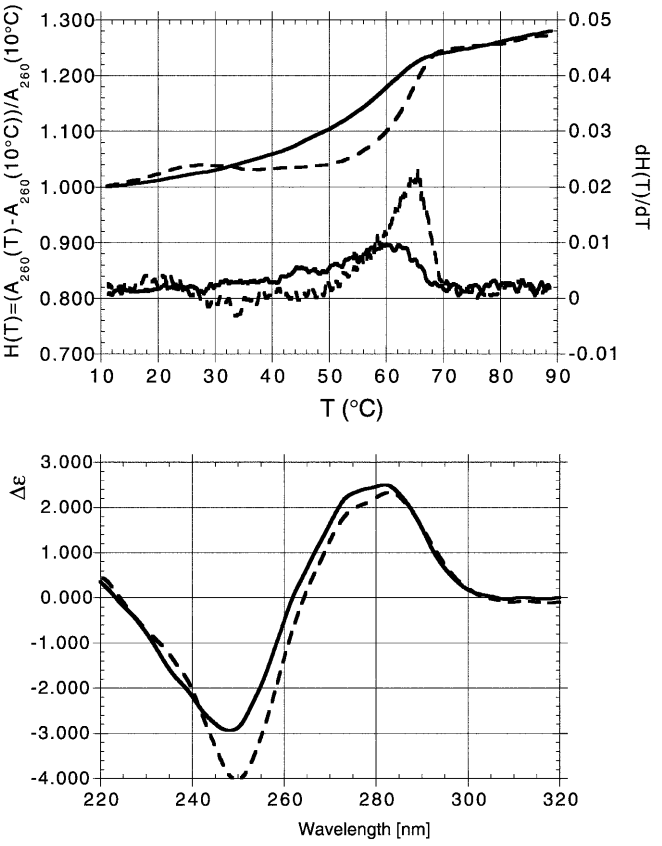


**Fig. 2** Thermal denaturation curves and derivatives (*upper panel*) and CD spectra (*lower panel*) of S100 (*solid line*) and C100 (*dashed line*) measured in 10 mM Na-cacodylate buffer

## FPA measurements

### *Two classes of FPA spectra*

The phase shifts of the straight fragments (Fig. 3) increase with the modulation frequency and at $\nu \approx 10$–$15$ MHz reach a maximum that depends on the number of DNA base pairs: the shorter the DNA, the larger the phase shift. A comparison of the two families of fragments is given in Fig. 4, where the phase shifts and the modulation ratios of the pairs of fragments (S100, C100 and S31, C31) are shown. While for the straight fragments the phase shifts clearly decrease at frequencies above the peak, the curved fragments either exhibit a much less pronounced decrease or reach a plateau value in this region. Beside the peculiar behavior of the phase shifts at high frequencies, one also notices that the modulation ratios of the C100 fragment are systematically lower than those of the S100; much smaller differences are observed for the other couple (S31, C31), probably due to the small size of the fragment. Similar behavior is observed for other pairs of fragments of equal length belonging to the S and the C families. Therefore, the different behavior of the FPA data seems to correlate with the predicted "anomalous" structure of the fragments.

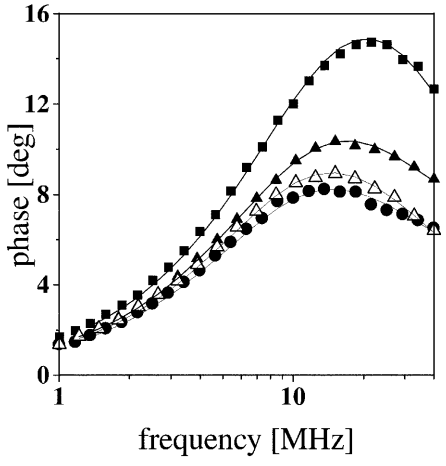


**Fig. 3** FPA phase shifts measured for the S family of fragments, i.e. S31 (■), S80p (▲), S100p (Δ), and S106 (●), with 31, 80, 100, and 106 base pairs. The *solid lines* are the best fit with a straight cylinder model with torsional rigidity $\alpha = 8 \times 10^{-12}$ erg and persistence length $P = 200$ nm

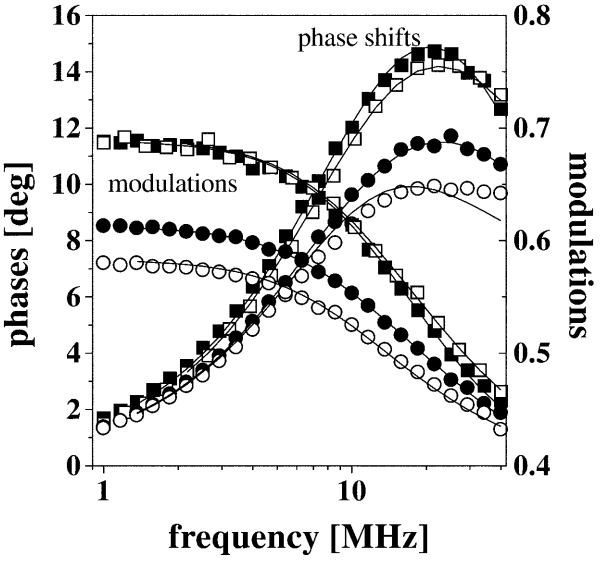


**Fig. 4** Phase shifts and modulation ratios for the fragments S31 (■), C31 (□), S100 (●), and C100 (○). The *solid lines* indicate the best fits from a straight cylinder model with torsional rigidity $\alpha = 8 \times 10^{-12}$ erg, persistence length $P = 200$ nm, and the hydrodynamic radii reported in Table 1

The fragments belonging to the S family can be successfully fit to a straight-rod model. Examples of the fit accuracy are given in Fig. 3 for the S31, S80p, S100p, and S106 fragments. The solid lines are best fit curves corresponding to a hydrodynamic radius $R_h = 10 \pm 1$ Å. Averaging over all the S family, one obtains $R_h = 9.5 \pm 1.4$ Å with $\chi^2 \approx 1.5$.

On the other hand, the DNAs of the C family cannot be successfully analyzed by the same straight cylinder model even when varying the torsional constant, α, and the dynamic persistence length, $P_{dyn}$, as free parameters of the fit. An example of FPA data taken on the C100 fragment is given in Fig. 4 together with data from the S100 "straight" fragment for comparison.

### *$R_h$ and $r_0$ are the most important parameters influencing the FPA spectra*

In order to understand the origin of the behavior of the curved sequences we have simulated FPA decays for different values of the global hydrodynamic radius, $R_h$, the limiting anisotropy, $r_0$, and the torsional constant, α. Figure 5 shows that the largest effect in the low-frequency region ($\nu < 10$–15 MHz) is due to the change of the hydrodynamic radius and of the limiting anisotropy; the data are not very sensitive to the torsional constant. The effect of DNA length shown in the upper panel indicates that small errors (< 10%) in the length of the fragments do not affect appreciably the FPA data. However, comparing these simulations to the experimental findings (see Figs. 3 and 4) still offers no straightforward explanation for the "anomalous" features of the spectra of the curved fragments at high frequencies.

### *FPA spectra of curved fragments can be fitted by the straight cylinder model in the low-frequency region*

From Fig. 5 one also realizes that the hydrodynamic radius can be determined much more precisely by analyzing the lower frequency part of the spectra, since the torsional constant α is not affecting the experimental data at $\nu < 10$ MHz very much. We have therefore analyzed the spectra of all fragments in the frequency region $1.2 < \nu < 12$ MHz, leaving the hydrodynamic radius and the limiting anisotropy as free fitting parameters (see Table 2). The torsional constant α has been kept at $\alpha = 8 \times 10^{-12}$ erg; however, the quality of the fit was almost insensitive to the value chosen for α (data not shown). The data of all the fragments can be fit satisfactorily, and the best fit $R_h$ and $r_0$ values are reported in Table 2. The limiting anisotropy, $r_0$, does not vary appreciably and is found to be $r_0 = 0.36 \pm 0.02$. The average values of the hydrodynamic radii over the straight and curved fragments are slightly but systematically different: $R_h = 9.7 \pm 1.3$ Å and $R_h = 11.3 \pm 1.3$ Å for the two sets of fragments (see Table 2). For the S family, the average value of the hydrodynamic radius from the fit in the low-frequency region is $R_h = 9.7 \pm 1.3$ Å. This is in excellent agreement with the value from a fit up to 40 MHz of modulation frequency, $R_h = 9.5 \pm 1.4$ Å, and confirms the validity of the low-frequency fit.

### *A larger hydrodynamic radius is compatible with curved structures of the DNA*

The ratios of the hydrodynamic radii of curved and straight DNAs with similar lengths, i.e. C31/S31, C100/

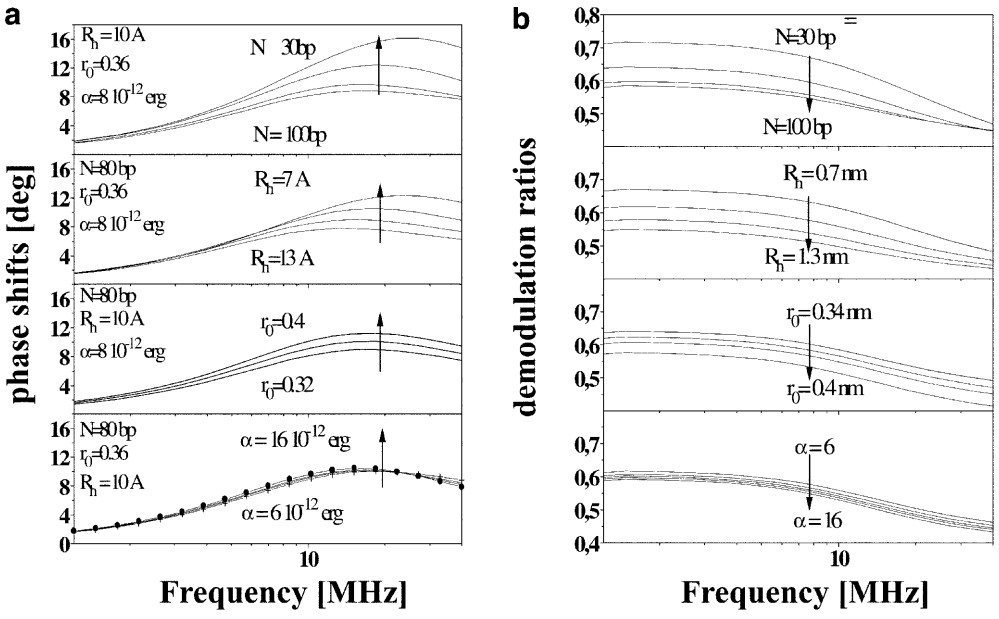


**Fig. 5** Simulations of the phase shifts (**a**) and demodulation ratios (**b**) for different choices of the DNA dynamical and geometrical parameters: length $30 < N < 100$ bp, hydrodynamic radius $7 < R_h < 13$ Å, zero-time anisotropy $0.34 < r_0 < 0.4$, and torsional constant $6 \times 10^{-12} < \alpha < 16 \times 10^{-12}$ erg

**Table 2** Best fit values of the analysis of the low-frequency part of the spectra ($v < 12$ MHz). The last column reports the ratio of the hydrodynamic radii of curved to straight fragments with similar length

| F name | Bp | Curvature | $r_0$ | $R_h$ [Å] | $\chi^2$ | $R_{cur}/R$ |
|---|---|---|---|---|---|---|
| S31 | 31 | N | 0.36 | 11.1 | 2.6 | – |
| S100 | 100 | N | 0.38 | 8.0 | 1.0 | – |
| S106p | 106 | N | 0.38 | 9.6 | 5.5 | – |
| Average | – | – | – | 9.7 | – | – |
| Standard dev. | – | – | – | 1.3 | – | – |
| C31 | 31 | Y | 0.33 | 12.2 | 5.2 | 1.1 |
| C100 | 100 | Y | 0.36 | 9.8 | 0.7 | 1.2 |
| C111p | 111 | Y | 0.37 | 12.0 | 1.5 | 1.3 |
| Average | – | – | – | 11.3 | – | – |
| Standard dev. | – | – | – | 1.3 | – | – |

S100, and C111p/S106p, are ~1.1, 1.2, and 1.3 (see Table 2). In order to understand this result, we must consider that a small curvature of the helix axis would induce an effective larger DNA radius in FPA measurements which are sensitive mainly to the overall spinning diffusion motions of the fragment. A curved DNA would have a lower spinning diffusion coefficient due to the larger expanse in the direction perpendicular to the average long DNA axis. This reduced spinning diffusion coefficient can then be interpreted by a fitting procedure in terms of a slightly larger DNA radius.

Simulations of the rotational diffusion coefficients of bent rods, as explained in the Materials and methods section, indicate that for a 20° bending angle the tumbling coefficient changes by about 1–4%, while the spinning diffusion decreases by 10–35% (Fig. 6). This would suggest that the ca. 10–30% change observed in the apparent hydrodynamic radius obtained by FPA is almost completely due to the change in the spinning diffusion.

Before resorting to more accurate numerical computation of the spinning diffusion coefficient of the DNA fragments, it is interesting to give an intuitive prediction of the dependence of the spinning diffusion coefficient upon the bending angle. Since a measure of the inertia related to rotational motions of a rigid body around an axis is given by its momentum of inertia around this axis, $I$, we can estimate an effective radius, $R$, by comparing the momentum of inertia, $I_S$, of the straight cylinder to that of the bend rod, $I_B$, of equal mass $M$. The first is computed around the cylinder symmetry axis and is given by $I_S = MR^2/2$. For a bent rod the spinning

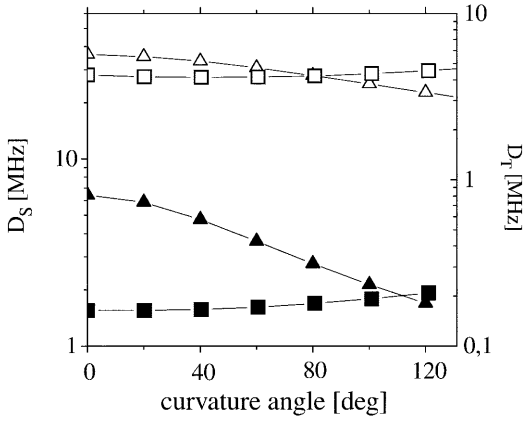


**Fig. 6** Tumbling (*squares*) and spinning (*triangles*) diffusion coefficients simulated as described in the text for 31 bp (*open symbols*) and 100 bp (*solid symbols*) DNA fragments with a central kink as a function of curvature angle. The curvature angle is the angle of a circular arc passing through the end points and the central joint of the fragment

motion occurs around an axis passing through the center of mass of each of the rod segments, and the momentum of inertia can be computed for small bending angles, $\theta$, as $I_B \approx MR^2/2 + \tan(\theta/2)^2 ML^2/48$. By comparing the two expressions, one defines an effective radius for small bending angles, $R_{eff}^2 \approx R^2 + \theta^2 L^2/96$, which is not exactly equal to the DNA hydrodynamic radius measured by fitting the FPA spectra, but is expected to depend upon the bending angle in a similar fashion. As an example we consider the 31 bp fragments, for which the ratio of the hydrodynamic radii obtained by the analysis of the FPA data is ca. 1.1 and the length is ca. 100 Å, giving $\theta \approx 25°$ for the bending angle. This value is less than our previous estimate, $\theta \approx 44°$, made on the same sequence at this salt concentration by means of fluorescence resonance energy transfer (FRET) (Tóth et al. 1998). The reason for the deviation between the two methods might be first of all the higher uncertainty of the FPA analysis; second, in the case of a dynamic equilibrium between strongly and weakly bent structures, shorter distances are given more weight in FRET owing to the $R^{-6}$ dependence of the energy transfer.

The simple estimate of the bending angle is confirmed by the more precise calculation using the hydrodynamic model described in the Materials and methods section. Table 1 compares the calculated spinning and tumbling rotational diffusion coefficients for the DNA structures predicted from the Bolshoy model with the experimental ones. The agreement is quite good for the 31 and 80 bp fragments; the theoretical spinning coefficients for the 100 and 110 bp fragments are, however, much smaller than the measured ones. This shows that the deviations from the rigid shape due to Brownian motion become important here and lead to a structure that is on the average less expanded about the long axis than a rigid shape would be.

### *The high-frequency part of the spectra of the curved fragments suggests non-uniform dynamic properties of the DNAs*

The FPA spectra at high frequencies, particularly the plateau of the phase shift at $\nu > 15$ MHz, indicate an additional faster relaxation mode in the FPA decay. From the simulations reported in Fig. 7 one can see that these spectral features cannot be explained by anomalous values of basic DNA parameters such as hydrodynamic radius or elastic constants. A possible way to describe the experimental trends appears to be a non-uniform elasticity of the fragment. We have tested this hypothesis by considering a simplified model of a flexible torsional and/or bending joint.

In this case, in addition to the DNA torsional constant, $\alpha$, length, $L$, and radius, $R_h$, two more parameters are introduced, namely the bending and torsional variances of the angular displacements of the dye due to the relative motion of the DNA about the joint. It must be stressed that this is only an approximate and simplistic

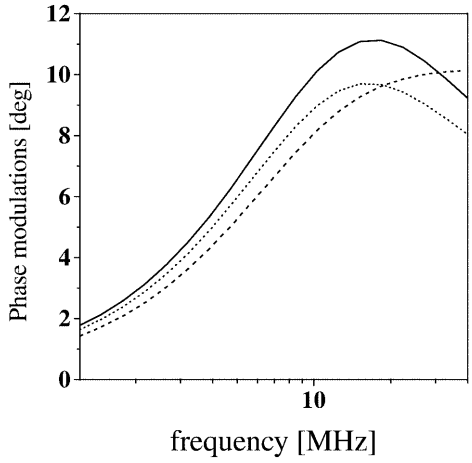


**Fig. 7** Simulations of the phase shifts for a 31 bp straight DNA fragment (*solid line*) and with a torsional ($\sigma_T = 0.3$, *dashed line*) or bending ($\sigma_B = 0.3$, *dotted line*) joint in the center of the structure

model for some anomaly in the elastic properties of a short DNA fragment in the center of its structure. We can easily estimate the effect of such an anomaly on the FPA spectra by simulating the decay for a purely torsional joint, i.e. $F_{j,n}(t) = 1$, or a purely bending joint, i.e. $C_{j,n}(t) = 1$. From Fig. 7 one can see that while the bending joint simply increases the phases towards higher values, the torsional joint induces a leveling off of the data at higher frequencies, very similar to what is found experimentally.

In conclusion, we have brought into evidence a small but systematic increase in the apparent hydrodynamic radius of DNA fragments which correlates positively with helix axis curvature predicted by computer simulations or from gel migration anomaly. It is noteworthy that our results from fit with a straight cylinder at $\nu < 15$ MHz, though mostly qualitative, put into evidence the presence of curvature *in solution*. Moreover, by comparing the whole FPA decay with a simple approximate model, we suggest that the source of the anomalous behavior at higher frequencies, shown by some fragments with bent structure analyzed here, may be due to enhanced torsional flexibility of these molecules.

**Acknowledgement** This work was supported by NATO collaborative research grant CRG 910239.

## References

Barkley MD, Zimm BH (1979) Theory of twisting and bending of chain macromolecules: analysis of the fluorescence depolarization of DNA. J Chem Phys 70: 2991–3007

Bolshoy A, McNamara P, Harrington RE, Trifonov EN (1991) Curved DNA without A-A: experimental estimation of all 16 DNA wedge angles. Proc Natl Acad Sci USA 88: 2312–2316

Bracco L, Kotlarz D, Kolb A, Diekmann S, Buc H (1989) Synthetic DNA curved sequences can act as transcriptional activators in *E. coli*. EMBO J 8: 4289–4296

Chan SS, Breslauer KJ, Hogan ME, Kessler DJ, Austin RH, Ojemann J, Passner JM, Wiles NC (1990) Physical studies of DNA premelting equilibria in duplexes with and without homo dA.dT tracts: correlations with DNA bending. Biochemistry 29: 6161–6171

Chan SS, Breslauer KJ, Austin RH, Hogan ME (1993) Thermodynamics and premelting conformational changes of phased (dA)5 tracts. Biochemistry 32: 11776–11784

Chan SS, Austin RH, Mukerji I, Spiro TG (1997) Temperature-dependent ultraviolet resonance Raman spectroscopy of the premelting state of dA.dT DNA. Biophys J 72: 1512–1520

Collini M, Chirico G, Baldini G (1992) DNA torsional dynamics by multifrequency phase fluorometry. Biopolymers 32: 1447–1459

Collini M, Chirico G, Baldini G, Bianchi ME (1995) Conformation of short DNA fragments by modulated fluorescence polarization anisotropy. Biopolymers 36: 211–225

Collini M, Chirico G, Baldini G, Bianchi ME (1998) Enhanced flexibility of a bulged DNA fragment from fluorescence anisotropy and Brownian dynamics. Macromolecules 31: 695–702

Diekmann S (1986) Sequence specificity of curved DNA. FEBS Lett 195: 53–56

Doi M, Edwards SF (1986) The theory of polymer dynamics. Oxford University Press, Oxford

Eimer W, Pecora R (1991) Rotational and translational diffusion of short rodlike molecules in solution: oligonucleotides. J Chem Phys 94: 2324–2329

Fujimoto BS, Miller JM, Ribeiro S, Schurr JM (1994) Effects of different cations on the hydrodynamic radius of DNA. Biophys J 67: 304–308

García Bernal JM, García de la Torre J (1980) Transport properties and hydrodynamic centers of rigid macromolecules with arbitrary shapes. Biopolymers 19: 754–766

García de la Torre J, Navarro S, López Martínez MC, Díaz FG, López Cascales JJ (1994) HYDRO: a computer software for the prediction of hydrodynamic properties of macromolecules. Biophys J 67: 530–531

García de la Torre J, Carrasco B, Harding SE (1997) SOLPRO: theory and computer program for the prediction of SOLution PROperties of rigid macromolecules and bioparticles. Eur Biophys J 25: 361–372

Griess EA, Grasser KD, Feix G (1993) Repeat units from a maize rDNA external spacer region exhibit DNA curvature and interact with high-mobility-group proteins. Planta 191: 524–531

Hammermann M, Steinmaier C, Merlitz H, Kapp U, Waldeck W, Chirico G, Langowski J (1997) Salt effects on the structure and internal dynamics of superhelical DNAs studied by light scattering and Brownian dynamics. Biophys J 73: 2674–2687

Kim J, Klooster S, Shapiro DJ (1995) Intrinsically bent DNA in a eukaryotic transcription factor recognition sequence potentiates transcription activation. J Biol Chem 270: 1282–1288

Kremer W (1992) Hydrodynamische Charakterisierung von superhelikaler DNA und DNA-Fragmenten. Doctoral thesis, University of Göttingen

Kremer W, Klenin K, Diekmann S, Langowski J (1993) DNA curvature influences the internal motions of supercoiled DNA. EMBO J 12: 4407–4412

Lakowicz JR (1983) Principles of fluorescence spectroscopy. Plenum Press, New York

Lakowicz JR, Maliwal BP (1985) Construction and performance of a variable-frequency phase-modulation fluorometer. Biophys Chem 21: 61–78

Längst G, Schätz T, Langowski J, Grummt I (1997) Structural analysis of mouse rDNA: coincidence between nuclease hypersensitive sites, DNA curvature and regulatory elements in the intergenic spacer. Nucleic Acids Res 25: 511–517

Laundon CH, Griffith JD (1988) Curved helix segments can uniquely orient the topology of supertwisted DNA. Cell 52: 545–549

Lavigne M, Herbert M, Kolb A, Buc H (1992) Upstream curved sequences influence the initiation of transcription at the *Escherichia coli* galactose operon. J Mol Biol 224: 293–306

Levene SD, Wu HM, Crothers DM (1986) Bending and flexibility of kinetoplast DNA. Biochemistry 25: 3988–3995

Ohyama T (1996) Bent DNA in the human adenovirus type 2 E1A enhancer is an architectural element for transcription stimulation. J Biol Chem 271: 27823–27828

Perez-Martin J, Timmis KN, de Lorenzo V (1994) Co-regulation by bent DNA: functional substitutions of the integration host factor site at sigma(54)-dependent promoter Pu of the upper-TOL operon by intrinsically curved sequences. J Biol Chem 269: 22657–22662

Pfannschmidt C, Langowski J (1998) Superhelix organization by DNA curvature as measured through site-specific labeling. J Mol Biol 275: 601–611

Pörschke D, Schmidt ER, Hankeln T, Nolte G, Antosiewicz J (1993) Structure and dynamics of curved DNA fragments in solution: evidence for slow modes of configurational transitions. Biophys Chem 47: 179–191

Rojo F, Salas M (1991) A DNA curvature can substitute phage phi29 regulatory protein p4 when acting as a transcriptional repressor. EMBO J 10: 3429–3438

Schätz T, Langowski J (1997) Curvature and sequence analysis of eukaryotic promoters. J Biomol Struct Dyn 15: 265–275

Schurr JM (1984) Rotational diffusion of deformable macromolecules with mean local cylindrical symmetry. Chem Phys 84: 71–96

Schurr JM, Fujimoto BS, Wu P, Song L (1992) Fluorescence studies of nucleic acids: dynamics, rigidities and structures. In: Lakowicz JR (ed) Topics in fluorescence spectroscopy, vol 3. Plenum Press, New York, pp 137–229

Song L, Schurr JM (1990) Dynamic bending rigidity of DNA. Biopolymers 30: 229–237

Song L, Fujimoto BS, Wu PG, Thomas JC, Shibata JH, Schurr JM (1990) Evidence for allosteric transitions in secondary structure induced by superhelical stress. J Mol Biol 214: 307–326

Thomas JC, Allison SA, Appellof CJ, Schurr JM (1980) Torsion dynamics and depolarization of fluorescence of linear macromolecules. II. Fluorescence polarization anisotropy measurements on a clean viral phi 29 DNA. Biophys Chem 12: 177–188

Tirado MM, García de la Torre J (1979) Translational friction coefficients of rigid, symmetric top molecules. Application to circular cylinders. J Chem Phys 71: 2581–2587

Tirado MM, García de la Torre J (1980) Rotational dynamics of rigid, symmetric top molecules. Application to circular cylinders. J Chem Phys 73: 1986–1993

Tóth K, Sauermann V, Langowski J (1998) DNA curvature in solution measured by fluorescence resonance energy transfer. Biochemistry 37: 8173–8179

Trifonov EN, Sussman JL (1980) The pitch of chromatin DNA is reflected in its nucleotide sequence. Proc Natl Acad Sci USA 77: 3816–3820

Tsen H, Levene SD (1997) Supercoiling-dependent flexibility of adenosine-tract-containing DNA detected by a topological method. Proc Natl Acad Sci USA 94: 2817–2822

Weber G (1977) Theory of differential phase fluorometry: detection of anisotropic molecular rotations. J Chem Phys 66: 4081–4091

Wu P, Fujimoto BS, Schurr JM (1987) Time-resolved fluorescence polarization anisotropy of short restriction fragments: the friction factor for rotation of DNA about its symmetry axis. Biopolymers 26: 1463–1488